IEEE Access
Multidisciplinary | Rapid Review | Open Access Journal

Received May 22, 2020, accepted June 2, 2020, date of publication June 5, 2020, date of current version June 17, 2020.

Digital Object Identifier 10.1109/ACCESS.2020.3000227

An Infrared Small Target Detection Algorithm Based on Peak Aggregation and Gaussian Discrimination

YUHANG JIANG[1], LILI DONG[2], (Member, IEEE), YANG CHEN[2], AND WENHAI XU[2]
[1]Naval Architecture and Ocean Engineering College, Dalian Maritime University, Dalian 116000, China
[2]Information Science and Technology College, Dalian Maritime University, Dalian 116000, China

Corresponding author: Lili Dong (donglili@dlmu.edu.cn)

This work was supported in part by the National Natural Science Foundation of China under Grant 61701069, and in part by the Fundamental Research Funds for the Central Universities of China under Grant 3132019340 and Grant 3132019200.

ABSTRACT Due to its inherent characteristics, infrared small target detection plays an important role in the field of image detection. In order to improve the detection accuracy of small infrared targets under complex sea background, by analyzing the difference between small targets and sea clutter, we propose an infrared small target detection algorithm based on the peak aggregation number and Gaussian discrimination. First we remove the background through local large value detection and extracts suspect targets. Then, the peak aggregation number of the suspected target is counted to eliminate most of the strong wave clutter and strong island edges. Finally, the small waves are eliminated by Gaussian discrimination. The experimental results show that our algorithm has good performance under strong noise interference and calm sea conditions.

INDEX TERMS Target detection, small infrared target, local large value, peak aggregation number, Gaussian discrimination.

I. INTRODUCTION

The infrared small target detection technology is one of the key technologies in the sea surface rescue system and early warning system. The accuracy of the detection method directly affects the performance of the application system. Due to the long detection distance and the influence of atmospheric transmission, the amount of target radiation received by the sensor is usually small and effective targets are easily submerged by noise and background wave clutter. It is extremely difficult to accurately detect effective targets [1]–[5]. Therefore, the detection of small infrared targets under complex backgrounds becomes a research hotspot now.

In general, infrared small target detection methods are mainly divided into two categories: detection based on single-frame (SF) and multi-frame (MF), respectively. SF detection is to use only one image to achieve the goal of target detection, while MF detection is to achieve the same goal by multiple images related to each other. Compared with SF algorithm, MF algorithm requires the targets between frames have a strong correlation and the background should be stable. These assumptions are difficult to meet in the actual detection environment due to the influence of severe sea and weather conditions. At the same time, because the MF algorithm needs to process multiple images to achieve detection, the complexity of these algorithms is usually high and it is difficult to meet the requirements of real-time detection. In addition, a large number of MF algorithms are implemented based on the results of SF detection. Therefore, compared with MF algorithms, SF algorithms usually have the advantages of low prior knowledge, strong real-time performance, and low hardware requirements. Therefore, we study the detection algorithms based on SF. Currently, SF detection can be divided into three types: detection based on target analysis, detection based on background suppression and detection based on statistics.

The algorithms based on target analysis focus on the analysis of target characteristics. By analyzing the target-background differences, corresponding algorithms are proposed to realize the detection of small infrared targets under complex backgrounds. For example, Chen *et al.* adopted a method based on local contrast, they used the brightness difference between the target and its neighboring area to detect the target [6]. Although this method is effective, it will be affected by high brightness noise [7]. Qi *et al.* regarded the

The associate editor coordinating the review of this manuscript and approving it for publication was Naveed Akhtar.

target as a salient area that is distinct from the background, and detected the target through salient area detection [4]. However, strong wave clutter is also more prominent in some cases, which will lead to a higher false alarm rate of the detection results. In 2016, Wei *et al.* proposed a new multiscale patch-based contrast measure for small infrared target detection, which can simultaneously enhance dark and light targets [8]. However, its robustness is not good enough under noisy and complex situations. In 2018, Nie *et al.* proposed a multiscale local homogeneity measure method by integrating the internal homogeneity of the target itself and increasing the heterogeneity between the target and local background regions [9]. This method also has low discrimination of strong clutter, which leads to a high false alarm rate. In short, due to the similarity characteristics between the high-brightness noise and the target and the analysis of the target characteristics is insufficient, in the background of strong wave clutters, the above algorithms all have a high false alarm rate.

Algorithms based on background suppression focus on the estimation of the background. On the basis of estimating the background, the small target is detected by the difference between the original image and the background. Most of these methods are implemented by filtering. Such as traditional algorithms: top-hat filtering [10], maximum mean filtering, maximum median filtering [13] and bilateral filtering [14], [15]. These methods are simple and efficient, and have a good detection effect on the simple background, but cannot accurately achieve the task of accurate detection under a complex background. Therefore, in recent years, domestic and foreign scholars have proposed several new algorithms for images with complex backgrounds. In [16], Hou and Zhang proposed the spectral residuals (SR) method. They transformed the image into a logarithmic domain and removed redundant backgrounds through the Fourier transform of the image. In order to obtain better background filtering effect, Liu and Li [17] proposed a soft morphology TopHat method, which combined the advantages of soft mathematical morphology filtering and TopHat filtering to solve the problem of point target detection. Hu *et al.* [2] proposed R-NLM, using a non-local mean (NLM) filter to estimate the original background. This method is based on local regularity and self-similarity theory, and achieves accurate background estimation and successful extraction of weak targets. These algorithms have been greatly improved compared with the traditional algorithms, But the background estimation methods described above are inadequate for the detection of weak point targets for the background of islands and strong wave clutter.

The statistics-based methods regard the infrared small target detection problem as a two-class pattern recognition task, mostly are based on massive data and implement using machine learning [18], [19]. Liu *et al.* [20] used the nonlinear principal component analysis (NLPCA) neural network (NN) to model the appearance of small objects and constructing a saliency measure function. Bi *et al.* [21] proposed multiple novel features from four aspects to establish elaborate description. Then, learning-based classifier is trained to screen candidate targets. Yang *et al.* [22] used the directional support value of Gaussian transform (DSVoGT) to enhance the targets and then trained the LS-SVM. Sparse representation has drawn strong research interests recently [23]. Zhao *et al.* [24] modeled a small target as a linear combination of certain target samples and then solved a sparse 0-minimization problem. Although the above methods can work well in complex background, the quality of selected features and training samples could evidently influence the detection results. Targets will not be well distinguished if the finite training samples are insufficient to involve enough information.

In order to obtain better performance under the complex sea surface background, we propose an infrared small target detection algorithm based on peak aggregation number and Gaussian discrimination. First, local large-value detection is performed, and pixels with higher gray levels in the local range are extracted as suspect targets. Then, based on local large-value detection, peak aggregation number is used to remove most of the strong wave clutter. Finally, the Gaussian discrimination is performed on the remaining suspect targets to obtain the most appropriate response. Experimental results show that the method can detect small infrared targets with high detection rate and low false alarms under complex background. The contributions of this paper can be summarized as follows:

- The similarities and differences between small targets and wave clutter are analyzed, which lays a theoretical foundation for effective extraction of small targets.
- The concept of peak aggregation number is proposed, which can clarify the difference between the internal grayscale characteristics of strong wave clutter and small targets in the image. The peak aggregation discrimination algorithm based on this criterion can effectively distinguish small targets with strong wave clutter.
- A Gaussian discriminant algorithm is proposed, which uses the structural characteristics of small targets as a detection condition. By analyzing the Gaussian characteristic of suspect targets, weak wave clutters can be effectively distinguished from small targets.

This article is organized as follows. The second part analyzes and demonstrates the difference between the small target and the wave clutter in detail. In the third part, an infrared small target detection algorithm based on the peak aggregation and Gaussian discrimination is proposed. The fourth part gives the experimental results and analysis. The fifth part summarizes the main work of this paper.

II. ANALYSIS OF WAVE CLUTTER AND TARGET CHARACTERISTICS

When the sea surface is calm, the difference between the small infrared targets and the background is large, and the effective detection of the target can be achieved by simple threshold judgment. But when there is a lot of wave clutter on the sea surface, the detection of small targets becomes

extremely difficult. The difficulty of small target detection under this complex background is that the wave clutter and the target have certain similarities. To accurately detect the small target, it is necessary to analyze the characteristics of the infrared small target and the wave clutter.

A. INFRARED SMALL TARGET CHARACTERISTICS

According to the research experience of previous scholars, most scholars regard small targets as internally homogeneous highlighted individuals [8], and believe that small targets have no shape characteristics. we consider this approximation is not comprehensive. The following figure lists four typical infrared small target images on the sea surface for analysis.

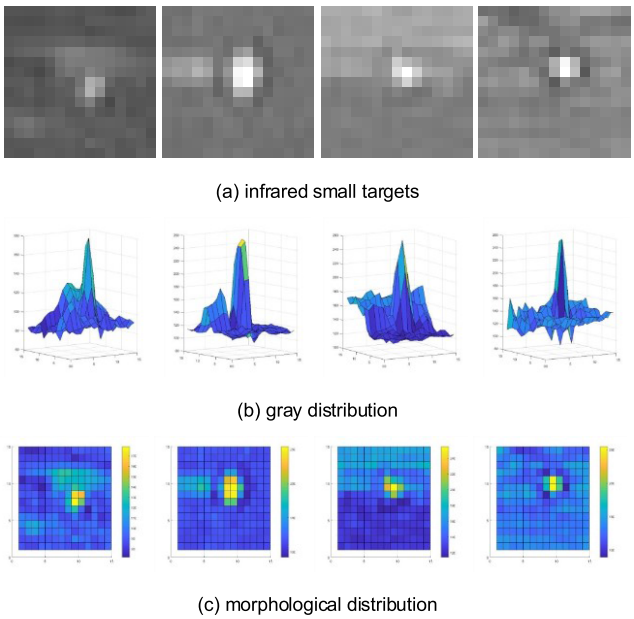

FIGURE 1. Infrared small target characteristics.

It can be seen from the figure above that the small target is locally significant compared with the background, and the gray distribution of the pixels inside the target is unbalanced and show a characteristic of approximate Gaussian distribution. In other words, there are a number of pixels with high gray scale and aggregation characteristics inside the target. The gray scale of these pixels is quite different from the surrounding pixels and with the increase of the distance from the max gray scale pixel, the gray scale value of the pixels along all directions decrease by roughly the same amount. We define the number of extremely high grayscale pixels in the locally significant region as the peak aggregation number and the shape characteristic caused by the isotropic grayscale attenuation is called Gaussian feature. Therefore, we believe that the characteristics of small infrared targets can be summarized as local salient, small peak aggregation number and Gaussian feature.

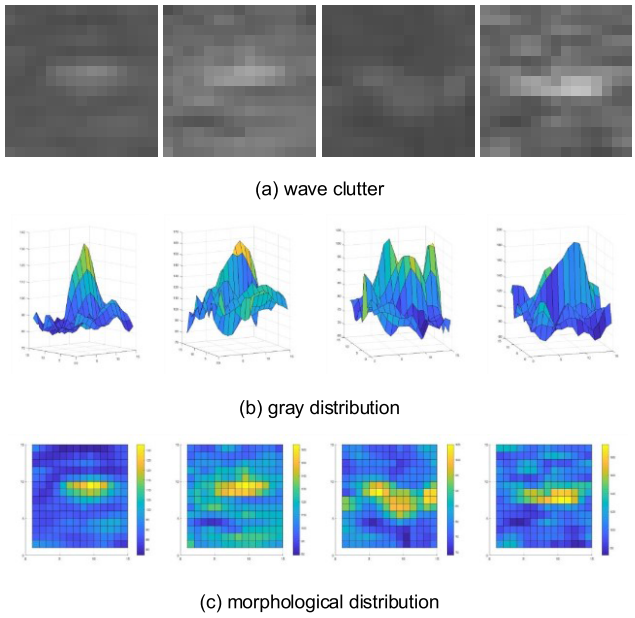

FIGURE 2. Wave clutter characteristics.

B. WAVE CLUTTER CHARACTERISTICS

Similar to small targets, sea clutter also shows local salient, which is the reason for the high false alarm rate of methods based on local contrast or local significance in complex backgrounds. Through analysis, we find that unlike small targets, the grayscale distribution of pixels in the wave clutters is more balanced, there are more pixels with high grayscale values than the targets'. We call this characteristic as large peak aggregation number. In addition, we also find that wave clutter has strong directivity, which is manifested as higher gray pixels of wave clutter with greater depth in the horizontal direction and rapid attenuation in the vertical direction. We define this property as the marginal. Therefore, we believe that the characteristics of wave clutter can be summarized as local salient, large peak aggregation number, and marginal.

III. ALGORITHM

Based on the above analysis, we propose a small infrared target detection algorithm based on peak aggregation and Gaussian discrimination. The algorithm is composed of three parts: local large value detection (LLVD), peak aggregation discrimination (PAD), and Gaussian discrimination (GaD). LLVD realizes the rough extraction of suspicious targets with the local significance of small targets as the standard. PAD realizes eliminating strong wave clutters with the small peak aggregation number of small targets as the standard; the GaD realizes eliminating the weak wave clutter with overall morphological structure of small targets as the standard.

A. LOCAL LARGE VALUE DETECTION

The implementation of LLVD: first we set a local detection window and calculate the average gray value of all pixels in

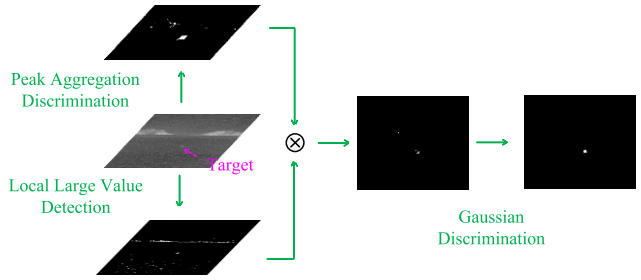

FIGURE 3. Infrared small target detection algorithm based on peak aggregation and Gaussian discrimination.

the window, then increase the average by λ and define this value as the local large value threshold Th_{LL}. The calculation of Th_{LL} is shown in formula (1).

$$Th_{LL} = \frac{\lambda}{L \times L} \sum_{m=i-floor(\frac{L}{2})}^{i+floor(\frac{L}{2})} \sum_{n=j-floor(\frac{L}{2})}^{j+floor(\frac{L}{2})} I(m,n) \qquad (1)$$

Among them, L is the size of the local detection window, $I(i,j)$ is the gray level of the pixel in the center of the window, λ is large value adjustment factor and Th_{LL} is the local large value threshold.

Then the central pixel point in the local window is discriminated based on Th_{LL}. If the central gray level is greater than Th_{LL}, a suspect area is formed, and the pixel point is retained, otherwise the pixel point is eliminated. The calculation is shown in formula (2).

$$result_{LL}(i,j) = \begin{cases} 1 & I(i,j) > Th_{LL} \\ 0 & I(i,j) < Th_{LL} \end{cases} \qquad (2)$$

$result_{LL}$ is the result of LLVD.

LLVD directly calculates the average gray value of the local area, and then increases λ times as a threshold parameter to extract the target. Compared with the method of maximum median filtering and maximum mean filtering, which first estimates the background, then uses the difference method to extract the suspect target area, finally perform threshold segmentation, our algorithm has lower complexity and higher detection efficiency. Compared with the traditional local peak method, because the local average gray is more stable relative to the local peak, the extraction effect of the algorithm is less restricted by the selection of the window size, which reduces the complexity of parameter analysis.

In different window sizes, we used three types of typical pictures: island interference image, high sea state image, and calm sea image to test the detection effects of the above four algorithms. Because the above four algorithms have a good extraction effect on the local salient area, and the target has local significance will definitely be detected, so we use the total number of pixels detected by different algorithms as the standard to evaluate the detection accuracy of these algorithms. The larger the total number of pixels detected, the lower the detection accuracy of the algorithm.

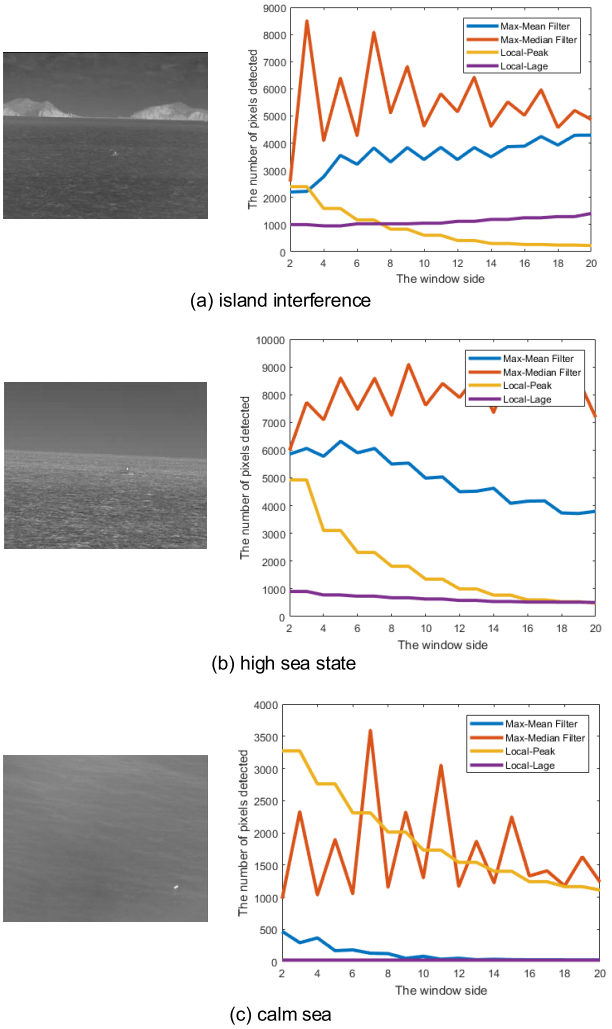

FIGURE 4. Extraction accuracy of maximum median filtering, maximum mean filtering, local peak and LLVD under different sea surface interference conditions.

It can be known from FIGURE 4. that the numbers of pixels detected by the maximum median filtering for the above three types of images are large, and show meaningless fluctuations with the change of the detection window. It means that maximum median filtering has low accuracy and low robustness. Maximum median filtering has better detection effect on calm sea images, but its detection accuracy is far from enough for complex sea surface just like (a) and (b). The detection results of local peak heavily depend on the size of the detection window. LLVD can maintain a low false detection rate in various scenarios, and the detection result is almost unaffected by window selection, which shows that LLVD is robust and accurate.

B. PEAK AGGREGATION DISCRIMINATION

After LLVD, a coarse extracted image containing small targets and a large amount of background noise can be obtained. The background noise is mainly composed of three parts:

strong wave clutter, weak wave clutter and island edges. If the image covers the sky area, the extracted noise maybe including clouds. The grayscale properties of the cloud and islands after imaging are roughly the same as the waves: the grayscale distribution of the internal pixels is uniform. Therefore, for the determination of peak aggregation, strong wave clutter, island edges and clouds can be considered as the same kind of noise. According to the analysis in Section 2, they are considered to be characterized by large peak aggregation number. Small targets are characterized by small peak aggregation number. Therefore, the PAD has a good ability to distinguish false targets such as strong waves, island edges and clouds from real small targets.

The PAD is as follows: first, we find the max grayscale value in the local area and attenuate it by a certain amount as the local peak threshold, as shown in formula (3):

$$Th_{i,j}^{Peak} = \max(I(p,q)) - a, \quad p \in [i - floor(L/2), i + floor(L/2)] \quad q \in [j - floor(L/2), j + floor(L/2)] \tag{3}$$

where $Th_{i,j}^{Peak}$ is the local peak threshold, I is the original image, (p, q) is the detection range, L is the size of the detection window, and a is the peak attenuation. After finding the local peak threshold, the number of pixels whose gray level is greater than the threshold is counted in the detection window, as shown in formula (4):

$$Num_{i,j}^{Peak} = sum(I(p,q) > Th_{i,j}^{Peak}), \quad p \in [i - floor(L/2), i + floor(L/2)] \quad q \in [j - floor(L/2), j + floor(L/2)] \tag{4}$$

$Num_{i,j}^{Peak}$, is the peak aggregation number of the pixels at (i, j) position.

Finally, through the threshold decision of peak aggregation number, we keep the pixels whose peak aggregation number is less than the threshold, as shown in formula (5):

$$result_{PAD}(i,j) = \begin{cases} 1 & 0 < Num_{i,j}^{Peak} < Th_{num} \\ 0 & else \end{cases} \tag{5}$$

Th_{num} is the peak aggregation threshold, $result_{PAD}$ is the result of PAD.

The rationality of this method: Firstly, according to the previous discussion in this section, the peak aggregation discrimination can distinguish strong wave clutter and small targets well, so it has a good rejection effect on false targets; Secondly, in the flat region, the local max gray value is not much different from the gray of other pixels in the region. When attenuation by the peak attenuation a, it can be considered the local peak is smaller than the gray of all pixels in the region. That means $Num_{i,j}^{Peak} \approx L^2$. Therefore, the discrimination of the peak aggregation number can also well remove the flat background.

But there is a problem with PAD: Compared to the size of the small target, a large candidate area will be extracted in the suspect target area, and the extraction result is not accurate enough. The reason for this problem is that in the state where small targets exist independently, starting from the peak point entering the window until it leaving, all points in this range are considered as target. In our algorithm, the sliding step size of the detection window is 1, that is, theoretically, PAD will detect a rectangular area containing the target. The size of this area mainly depends on the size of the window. Because we set the size of the detection window large (the window size will be discussed in Section 4), the size of detected area will be larger than the actual target. In fact, PAD detected a suspected area containing the target. At the same time, LLVD detected the precise shape of the target. The results of above two steps are binary. So we perform an AND operation on the detection results of PAD and LLVD to obtain accurate targets.

C. GAUSSIAN DISCRIMINATION

Through the above two steps of screening, most of the background noise can be eliminated. But weak wave clutter is characterized by the small number of pixels, so even if the gray distribution is uniform, it is also characterized as local significance and small peak aggregation number as small targets. It is still in the detection result. Therefore, according to the structural differencečžGaussian feature and marginal between the small target and weak wave clutter, we extract the small target more finely. Since the Gaussian function is isotropic, the grayscale accumulation of pixels in the horizontal direction within the target neighborhood should be approximately equal to the grayscale accumulation of the corresponding number of pixel points in the vertical direction. Weak wave clutter is marginal, so the gray accumulations in the above two directions in their neighborhoods should be quite different. The following figures show the horizontal and vertical pixel grayscale distribution of weak wave clutter and small targets in their neighborhoods:

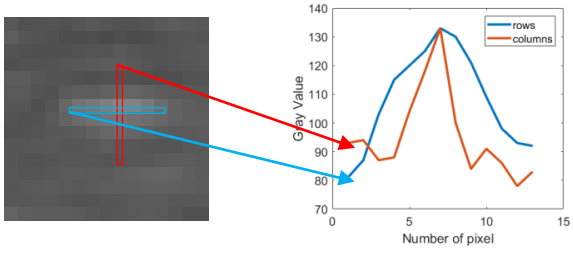

FIGURE 5. Horizontal and vertical pixel grayscale distribution of weak wave clutter.

As can be seen from the above figures, the grayscale distribution of small targets is Gaussian; while the weak wave clutter has edge nature, the grayscale distribution in the horizontal direction is greater than the vertical direction. Based on this difference in gray distribution, we define the Gaussian discrimination by the difference between the row gray accumulation and the column gray accumulation:

$$I_{GaD}(i,j) = \frac{\max(I_{RGA}(i,j), I_{CGA}(i,j))}{\min(I_{RGA}(i,j), I_{CGA}(i,j))} \tag{6}$$

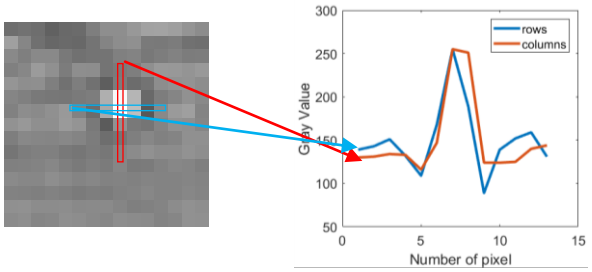

FIGURE 6. Horizontal and vertical pixel gray distributions of small target.

$$I_{RGA}(i,j) = \sum_{k=-n}^{n} I(i,j+k),\ I_{CGA}(i,j) = \sum_{k=-n}^{n} I(i+k,j) \tag{7}$$

$I_{RGA}(i,j)$ is the row gray accumulation amount of pixels located at the (i, j) position, $I_{CGA}(i,j)$ is the column gray accumulation amount of the corresponding position, and k is the gray accumulation range.

The judgment result is obtained by the following formula:

$$result_{GaD}(i,j) = \begin{cases} 1 & I_{GaD}(i,j) < Th_{GaD} \\ 0 & I_{GaD}(i,j) > Th_{GaD} \end{cases} \tag{8}$$

Among them, Th_{GaD} is the Gaussian discrimination threshold, $result_{GaD}$ is the result of GaD.

IV. PARAMETER ANALYSIS AND EXPERIMENT

A. PARAMETER ANALYSIS

There are many pending parameters involved in our algorithm, including the local detection window size L and the large value adjustment factor λ in the LLVD; the peak attenuation a and the peak aggregation threshold Th_{num} in the PAD; The gray-scale accumulation range k and the Gaussian discrimination threshold Th_{GaD} in GaD. This section will discuss and analyze these parameters one by one.

1) LOCAL DETECTION WINDOW SIZE

It can be known from FIGURE 4., that for different types of images, the size of the local detection window has little effect on the final detection result, and the number of detection results does not have a specific change law with the change of the window size. The purpose of LLVD is to find targets (including false targets) and extract morphology, positioning is achieved by PAD. So as long as the size of the detection window is larger than the size of the small target, the goal of suspicious target discovery can be achieved. The Optical Society of America defines a small target as a target having a size of less than 81 pixels [25]. Therefore, in order to be able to detect the target, L should be greater than 9. In order to ensure that the target is included, we add 2/3 of the maximum target as the window size. We set $L = 15$.

2) LARGE VALUE ADJUSTMENT FACTOR

The role of λ is to solve local large value threshold. When λ is set to be small, the local large value threshold is small, and the extracted image containing small targets contains more noise; otherwise, the extracted image contains less noise, but when the contrast of the target is low, it is easy to lose the target. Once the target is lost, it cannot be retrieved. Therefore, the choice of λ has a great impact on the final detection results and requires in-depth discussion.

We selected 130 infrared sea images of small targets and wave clutter, respectively, for analysis. The size of each image is 15 × 15 pixels, corresponding to the size of the local detection window L. We selected 26 images as examples, as shown in FIGURE 7.

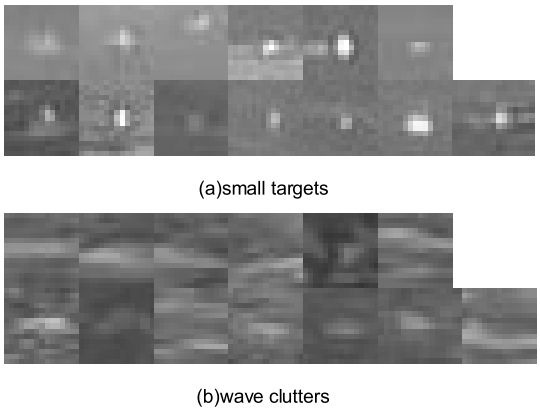

FIGURE 7. Small target and wave clutter images.

Because small targets and wave clutter are locally significant and only one type of target (small target or wave clutter) exists in our two types of images. Therefore, by changing λ, the targets (small target or wave clutter) in these two types of images are extracted by formula (1) and formula (2). As long as there are pixels with non-zero gray levels in the final image, it is considered that targets (small target or wave clutter) can be effectively extracted. The ultimate goal we want to achieve is to find an appropriate λ so that the detection results of LLVD can detect as less wave clutter as possible on the premise of extracting all small targets. We use the two types of data sets mentioned above to calculate the detection rates of small target and wave clutter respectively under different λ, as shown in FIGURE 8.

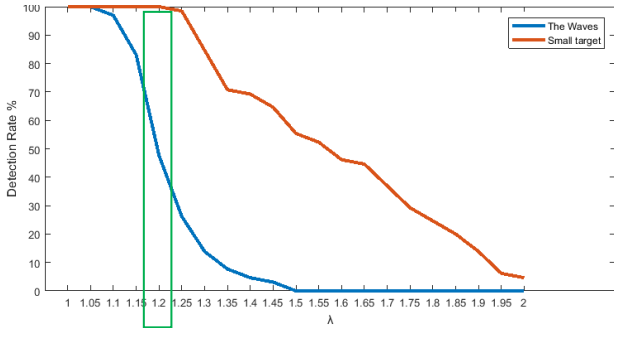

FIGURE 8. Targets and wave clutter detection rates for different λ.

As can be seen from the figure above, when $\lambda = 1.2$, the detection rate of small targets is 100%, and the detection rate of wave clutters is less than 50%. When λ increases,

the detection rate of wave clutters decreases significantly, but at the same time, the detection rate of small targets cannot be guaranteed to 100%. Because the subsequent processing steps can further reduce the false alarm rate, the retention of valid targets should be guaranteed during the LLVD stage. Therefore, based on the above analysis, we take λ as 1.2.

3) THRESHOLD OF PEAK AGGREGATION NUMBER

Th_{num} is an index used to describe the number of high pixel values. It divides the pixels in the small target into two categories, one is high gray value, the other is obvious gray value attenuation. Because the Optical Society of America defines a small target as a target smaller than 81 pixels in size [25], and the imaging characteristics of an ideal small target are consistent with Gaussianity, we analyze the value of Th_{num} combination with the size of the small target and its Gaussianity. The following figure is the normalized gray distribution of the two-dimensional Gaussian function. The size of the function is 9×9, the mean is 0, and the variance is 1.

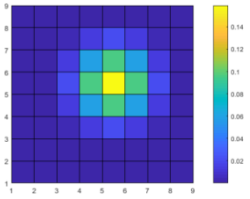

FIGURE 9. Gaussian function distribution.

As can be seen from the above figure, the main energy of the Gaussian function image is concentrated in a 3×3 square area in the central area, so the value of Th_{num} should be set to 9 in theory. In order to make the value of Th_{num} more convincing, we use the two types of data sets mentioned in Section 4.A.(2. to calculate the difference between the grayscale maximum value and the top 9 grayscale values, respectively, in each picture. Then we calculate the average and standard deviation (STD) of these differences. The resulting data is shown below.

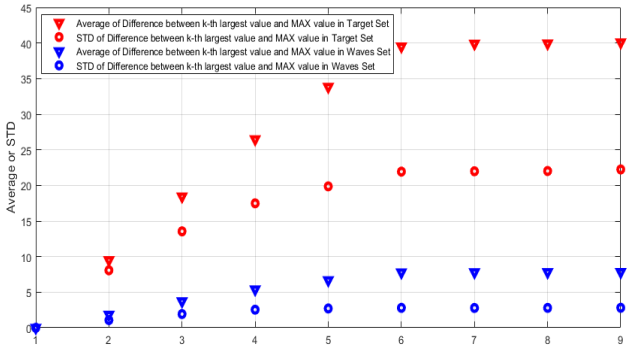

FIGURE 10. Statistical characteristics of the difference between k-th largest value and MAX value in two types of data sets.

According to the above figure, it can be clearly seen that, for small targets, the gray values of the top 5 pixels are larger than the rest. Moreover, the STD among the top 5 pixels is relatively small, which means that the degree of difference between each pixel is smaller. So compared to other pixels, these 5 pixels are singular. For the wave clutter, although it is consistent with the small target in the trend, its amplitude of average and STD are much smaller than the small target. Therefore, we take Th_{num} as 5.

4) PEAK ATTENUATION

The role of a is to find the local peak threshold. When a is set large, the local peak threshold is small and the peak aggregation number is large, the final extraction result contains more noise; Otherwise, the final extraction result contains less noise, but when the contrast of the target is low, it is easy to lose the target.

According to the analysis in Section 3.B., in order to eliminate flat areas, the larger the value of a the better. For wave clutter, the local gray level of it is quite balanced, so when the value of a is small, a large peak aggregation number can be obtained. If a is larger, the corresponding peak aggregation number will be larger; for small targets, when a is small, the local peak threshold is large, because of the gray value of the pixels around the small target has a large difference from the max value, the peak aggregation number will be extremely small. With the increase of a in a certain range, the peak aggregation number of the small target will be almost unchanged. From the discussion above, we think that the value of a should be relatively large.

After discussion in section 4.A.(3., we set Th_{num} to 5 as a basis, and this section will analyze the peak attenuation a. It can be known from the formula (3) that the local peak threshold is determined by the local gray max value and a. Therefore, we only need to determine the value of a, so that a should be larger than the difference between the max gray value and the 6th largest gray value in the target, smaller than the gray value difference of the corresponding pixel point in the wave clutter.

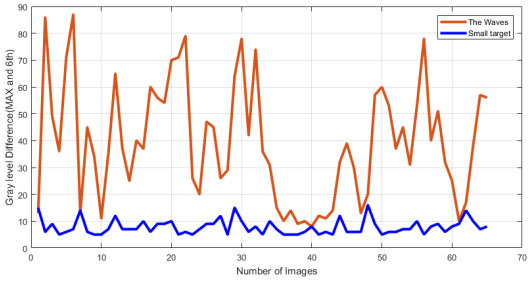

FIGURE 11. The difference between the max gray value and the sixth largest gray value in the small target and the wave clutter.

As can be seen from the above figure, when Th_{num} is set to 5, the difference between the grayscale max value and the sixth largest grayscale value of the wave clutter is within 15, and the grayscale difference corresponding to the pixels of the small target is distributed between 10 $\sim$ 85 and most of the targets have a gray difference greater than 15. So as long

as a > 15, the peak aggregation number of the waves will be greater than 6. But at the same time, a must not be too large. When a is too large, peak aggregation number of the target will be greater than 5, which will cause the loss of the real target. We use the following formula to solve a.

$$\begin{aligned} a &= \frac{1}{2}\left[(\mu_T - \sigma_T) - (\mu_w + \sigma_w)\right] + (\mu_w + \sigma_w) \\ &= \frac{1}{2}\left[(\mu_T - \sigma_T) + (\mu_w + \sigma_w)\right] \end{aligned} \tag{9}$$

where, μ_T is mean value of grey level difference for small target, σ_T is standard deviation of the same signal, μ_w and σ_w are corresponding parameters for wave clutter.

The rationality of formula (9) is that for the target, in order to increase the detection rate, it is required to reduce the peak aggregation number, so a should be small, therefore we subtract the standard deviation from the mean value of the target. In order to better eliminate the wave clutter, it is required to increase the peak aggregation number, so a should be larger, therefore we add the standard deviation to the corresponding mean value of the waves. Then find the difference and take 1/2. Finally add the expected value of the wave clutter, which means that we have established a threshold condition where the difference between the wave and the target is the largest. Through calculation, we get a $= 17.8$.

5) GRAY ACCUMULATION RANGE

Due to the first two stages: LLVD and PAD, most of the interference has been eliminated, so in the image to be processed at this stage, only a few suspicious regions are retained. Except for the suspected target area, the gray levels are all zero. Therefore, the size of k has little effect on the final extraction result, as long as k can cover the longest diameter (horizontal or vertical directions) of the target to be detected in the local area. In Section 4.A.1., we believe that $L > 9$ can meet the requirements, and setting L to 15 can guarantee to cover small targets. Because of the pre-processing, the requirements on the window coverage are reduced. In this section, in order to reduce the amount of computation and at the same time through experimental verification, we take k as 13.

6) GAUSSIAN DISCRIMINATION THRESHOLD

Th_{GaD} is another of the most important parameters in this paper. The final detection result is obtained after Th_{GaD} discrimination. The role of Th_{GaD} is to judge the similarity between the horizontal gray distribution and the vertical gray distribution of the suspected target. If the small target is an ideal imaging result, then $Th_{GaD} = 1$. Since there is no ideal imaging in practice, Th_{GaD} should be a number greater than and close to 1. If Th_{GaD} is too close to 1, the judgment criteria are too strict, and the probability of missed detection is greatly increased. If the Th_{GaD} is too large, the effect of reducing the false alarm rate will not be achieved. Therefore, the value of Th_{GaD} needs to be discussed and analyzed.

Use the two types of images in FIGURE 7 for analysis, and calculate the Gaussianity of the small targets and the wave clutters. We set the k to 13, and draw the result as a line chart as shown below.

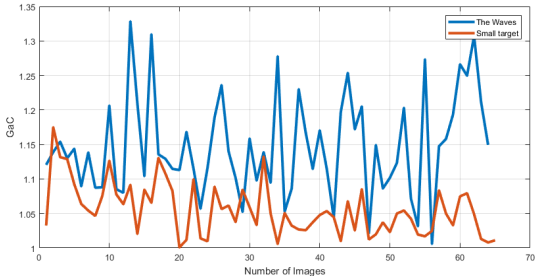

FIGURE 12. Gaussian difference between small targets and wave clutters.

Because the wave clutter and small target images used in this section are not extracted, that is, they contain background areas in addition to the wave clutters and small targets, the background area is gray-balanced and the gray value is not 0. In this case, Gaussian calculation results of the target have little effect. However, it has a greater impact on the result of the wave area, which will reduce the value of the Gaussianity of the wave clutter. The principle that causes this phenomenon is as follows:

$$R = \frac{A + C}{B + C} \tag{10}$$

when $A \approx B$ and $C = 0$, R is approximately equal to 1, in this case, if $C \neq 0$, the effect on R is small. When the difference between A and B is larger, if C is not equal to 0, the existence of C will cause R to approach 1.And in the algorithm of this paper, when calculating the Gaussianity, the gray values of all areas except the suspect target area are all 0, so $C = 0$ can be considered. Therefore, when the algorithm calculates the Gaussian, the Gaussian value of the wave clutter should be larger than the value in FIGURE 12. in this section, and the target's Gaussian value is basically unchanged.

We use the same method as formula (9) in Section 4.A.4. to calculate Th_{GaD} and get $Th_{GaD} = 1.08$. and through subsequent experiments (FIGURE 13.), it can be found that there are very few wave clutter in the GaD stage. Comprehensive analysis above, we set the Th_{GaD} to 1.1 at last.

B. EXPERIMENT

1) DETECTION RESULTS OF OUR ALGORITHM

After the parameters of the algorithm are determined, we use four types of images to verify the effectiveness of our algorithm. We list five sea surface images with complex backgrounds and one calm sea surface image, as shown in FIGURE 13., where the first and second are island interference images, the third and fourth are sea antenna interference images, the fifth is sea fog interference images, the sixth is a calm sea image.

From the above experimental results, it can be known that under complex backgrounds, the LLVD is relatively accurate in extracting the morphology of small targets, but there is a large amount of background noise; the PAD can more

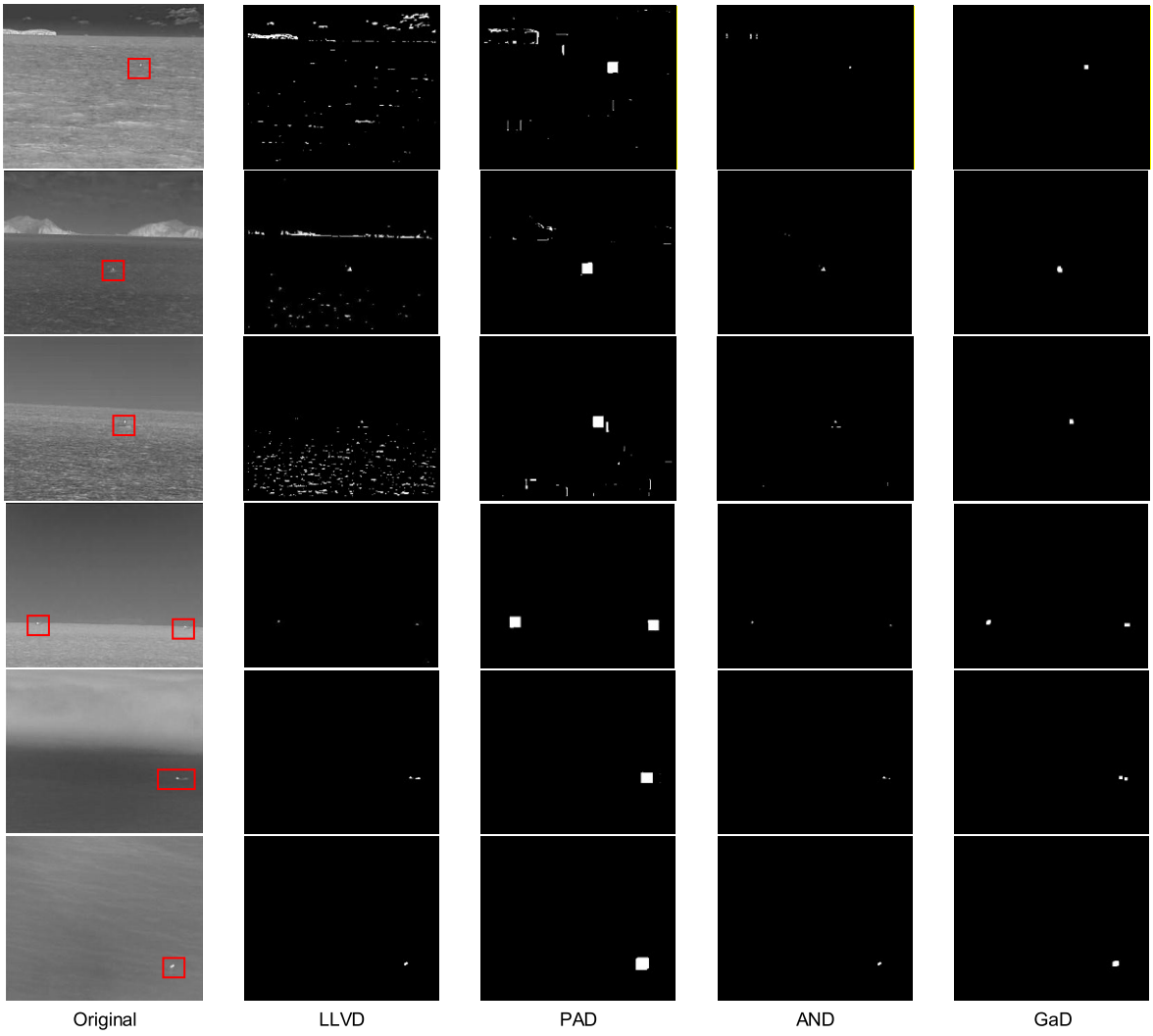

FIGURE 13. Experimental results of our algorithm. For easy observation, the results after GaD have undergone morphological expansion operation.

accurately locate the location of the target with less noise, but the coverage of small target detection results is large. After AND these two results, the image contains only a small amount of noise and small targets can be obtained. After the last step of the GaD, the residual noise is also removed, and only small targets exist in the image. The process proves that our method has a good detection effect on small infrared targets in a complex and calm sea backgrounds.

2) COMPARISON OF DIFFERENT ALGORITHMS

In order to illustrate the effectiveness of our algorithm, we conducted comparative experiments. The algorithm used are: Texture orientation-based algorithm for detecting infrared maritime targets (TO) [26], Infrared small target detection via non-convex rank approximation minimization joint l2,1 norm (NCL) [27], Multiscale patch-based contrast measure for small infrared target detection (MPCM) [18], Infrared small target detection based on local intensity and gradient properties (LIGP) [28]. The comparison detection results are shown in Figure 14.

For the three images: C, D, and E interfered by the sea antenna and fog, all algorithms can accurately detect the target without false targets. For the A affected by island interference, the detection results of NCL, MPCM, LIG and TO have different levels of noise interference. There are no false targets in detection results of our algorithm; for the multi-target image B of strong sea clutter interference, only our algorithm detects all targets. However there is some noise in the detection result of B, it can be found that a large amount of noise is distributed around the left-most target and a small amount of noise exists below the right-most target. In the original image, there is a dark band of low grayscale on the outer edge of the left-most target. The existence of this dark band reduces the local gray mean value, resulting in more pixel points being

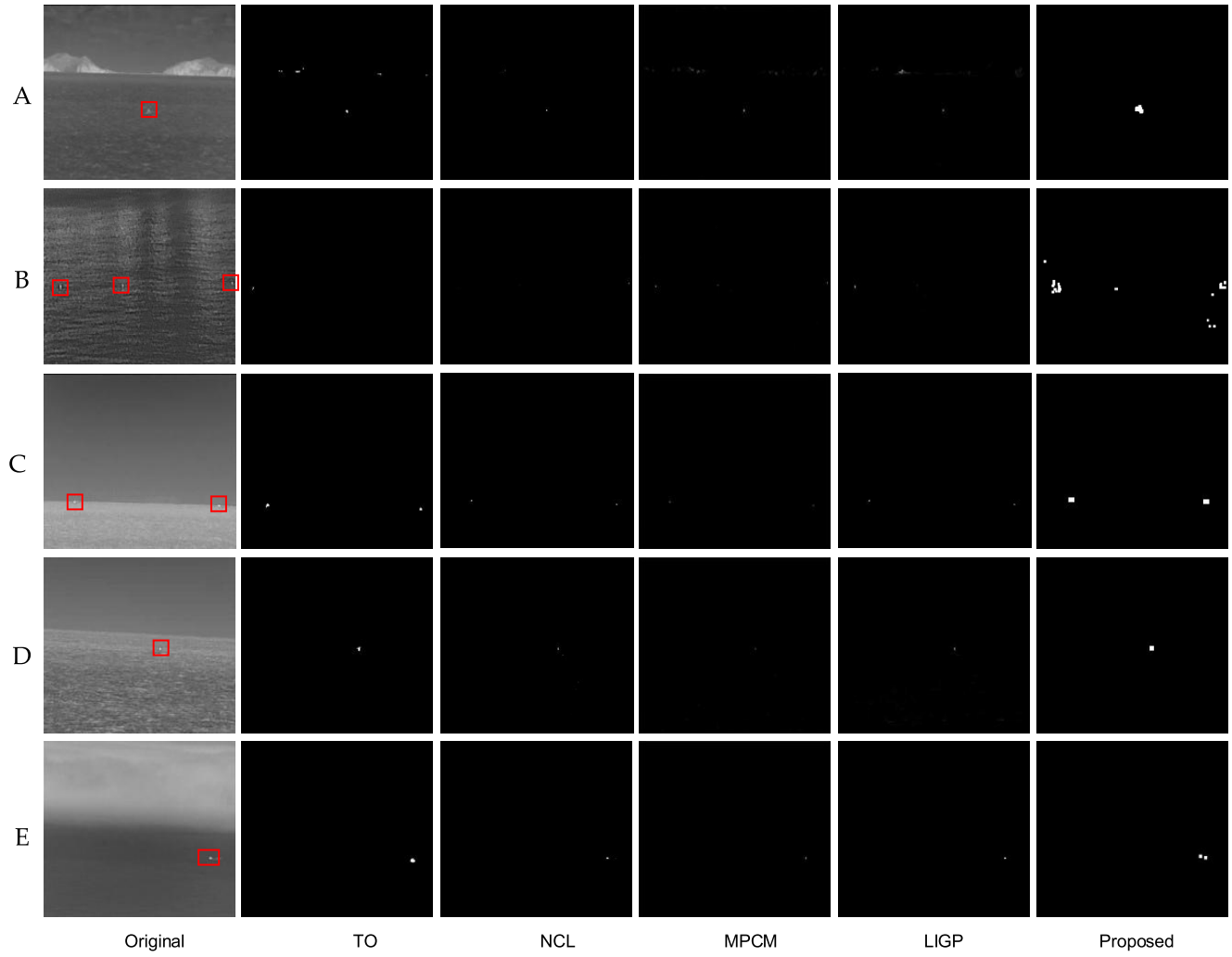

FIGURE 14. Comparison of detection results of different detection algorithms.

extracted in PAD. At the same time, since the target area detected by LLVD will be larger than the real target, the noise distributed around the real target will be retained, which eventually leads to the phenomenon of noise distribution around the target. In the actual detection mission, especially in the maritime search and rescue, the noise distributed around the target will not interfere with the final search. The target below the right-most target is detected because it is too similar to the target. On the premise of not knowing the real target, human eyes have the probability to confuse the truth and falsity of the right-most target and the target below, we believe that it is acceptable to detect such noise. Therefore the above experiments show that the detection results of our algorithm are accurate.

In order to more objectively judge the detection effect of our algorithm, we use four types of common sea surface scenes: island interference images A, sea antenna interference images B, calm sea images C, and sea fog interference images D to construct four data sets, each data set contains 50 images. Typical images of each type of data set are shown in FIGUURE 14.: (a), (b), (c), and (d) for quantitative analysis.

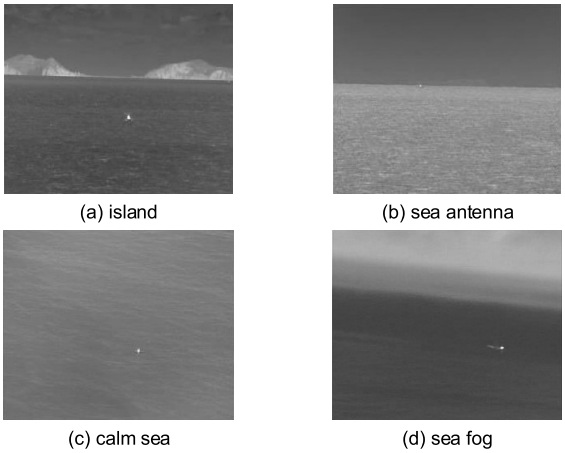

FIGURE 15. Typical images of four types of data sets.

TABLE 1. FAR of five detection algorithms.

		FAR(%)				
Data set	Number	Proposed	WTO	NCL	MPCM	LIGP
A	50	**9.8%**	10.3%	48.3%	22.4%	52.7%
B	50	**8.9%**	15.6%	33.8%	17.8%	83.8%
C	50	**0%**	0%	0%	0%	0%
D	50	**0%**	0%	0%	0%	0%
Total	200	**5.2%**	7.1%	21.5%	13.6%	42.5%

TABLE 2. MAR of five detection algorithms.

		MAR(%)				
Data set	Number	Proposed	WTO	NCL	MPCM	LIGP
A	50	**6.7%**	63.2%	6.7%	41.6%	6.7%
B	50	42.1%	87.5%	39.5%	67.9%	**4%**
C	50	**0%**	6.7%	0%	0%	0%
D	50	**5.9%**	24.6%	5.9%	5.9%	5.9%
Total	200	16.2%	59.2%	15.7%	47.5%	**2.7%**

TABLE 3. F1 score of five detection algorithms.

		F1				
Data set	Number	Proposed	WTO	NCL	MPCM	LIGP
A	50	**0.92**	0.52	0.66	0.67	0.31
B	50	**0.71**	0.22	0.63	0.46	0.28
C	50	**1**	0.97	1	1	1
D	50	**0.97**	0.86	0.97	0.97	0.97
Total	200	**0.89**	0.57	0.81	0.65	0.72

The evaluation index uses False Alarm Rate (FAR), Missed Alarm Rate (MAR) and F1 score. The definitions of FAR and MAR are shown in formulas (11), (12) and (13).

$$FAR = \frac{FD}{DT + FD} \times 100\% \tag{11}$$

$$MAR = \frac{MT}{DT + MT} \times 100\% \tag{12}$$

$$F1 = 2 \times \frac{(1 - FAR) \times (1 - MAR)}{(1 - FAR) + (1 - MAR)} \times 100\% \tag{13}$$

Among them, FD is the number of false targets detected, DT is the number of true targets detected, and MT is the number of small targets not detected. The statistical results are shown in Table 1, Table 2 and Table 3:

For FAR, our algorithm has the best detection results in various types of images, which shows that our algorithm has a good ability to remove false targets. For the MAR indicator, LIGP shows excellent detection performance, but it can be found from the comprehensive FAR indicator that the low MAR of LIGP is due to the existence of a large number of false targets in its detection results. It shows that the algorithm uses a strategy of increasing the FAR in exchange for a low MAR. This idea is of low value in practical applications, so it cannot explain the superiority of the performance of the algorithm. NCL also shows a similar phenomenon of high FAR and low MAR. Although the MAR index of our algorithm can not be the best among the five algorithms, according to the F1 score, we can get a conclusion that good trade-off between MAR and FAR is achieved, which proves the effectiveness of the algorithm in this paper.

V. CONCLUSION

This paper presents an infrared small target detection algorithm for complex sea background images based on peak aggregation and Gaussian discrimination. Firstly, by analyzing the characteristics of small targets and wave clutters on the sea surface, it lays a theoretical foundation for the proposed algorithm. Then elaborate the algorithm in this paper, based on the local saliency, the small number of peak aggregation, and the gray distribution of the Gaussian of the target, the LLVD, PAD, and GaD are proposed. Through step-by-step screening, various types of interference: flat background, strong wave clutters, island edges, and weak wave clutters can be effectively eliminated. Then detailed analysis and discussion are performed on each parameter of the algorithm. Finally, a large number of analysis experiments and comparative experiments illustrate the superior detection performance of the algorithm.

REFERENCES

[1] B. Wang, L. Dong, M. Zhao, and W. Xu, "Fast infrared maritime target detection: Binarization via histogram curve transformation," *Infr. Phys. Technol.*, vol. 83, pp. 32–44, Jun. 2017.
[2] J. Hu, Y. Yu, and F. Liu, "Small and dim target detection by background estimation," *Infr. Phys. Technol.*, vol. 73, pp. 141–148, Nov. 2015.

[3] S. Kim and J. Lee, "Scale invariant small target detection by optimizing signal-to-clutter ratio in heterogeneous background for infrared search and track," *Pattern Recognit.*, vol. 45, no. 1, pp. 393–406, Jan. 2012.
[4] S. Qi, J. Ma, C. Tao, C. Yang, and J. Tian, "A robust directional saliency-based method for infrared small-target detection under various complex backgrounds," *IEEE Geosci. Remote Sens. Lett.*, vol. 10, no. 3, pp. 495–499, May 2013.
[5] W. Meng, T. Jin, and X. Zhao, "Adaptive method of dim small object detection with heavy clutter," *Appl. Opt.*, vol. 52, no. 10, pp. D64–D74, 2013.
[6] C. L. P. Chen, H. Li, Y. Wei, T. Xia, and Y. Y. Tang, "A local contrast method for small infrared target detection," *IEEE Trans. Geosci. Remote Sens.*, vol. 52, no. 1, pp. 574–581, Jan. 2014.
[7] J. Han, Y. Ma, B. Zhou, F. Fan, K. Liang, and Y. Fang, "A robust infrared small target detection algorithm based on human visual system," *IEEE Geosci. Remote Sens. Lett.*, vol. 11, no. 12, pp. 2168–2172, Dec. 2014.
[8] Y. Wei, X. You, and H. Li, "Multiscale patch-based contrast measure for small infrared target detection," *Pattern Recognit.*, vol. 58, pp. 216–226, Oct. 2016.
[9] J. Nie, S. Qu, Y. Wei, L. Zhang, and L. Deng, "An infrared small target detection method based on multiscale local homogeneity measure," *Infr. Phys. Technol.*, vol. 90, pp. 186–194, May 2018.
[10] L. Deng, H. Zhu, Q. Zhou, and Y. Li, "Adaptive top-hat filter based on quantum genetic algorithm for infrared small target detection," *Multimedia Tools Appl.*, vol. 77, no. 9, pp. 10539–10551, May 2018.
[11] M. Zeng, J. Li, and Z. Peng, "The design of top-hat morphological filter and application to infrared target detection," *Infr. Phys. Technol.*, vol. 48, no. 1, pp. 67–76, Apr. 2006.
[12] X. Bai and F. Zhou, "Analysis of new top-hat transformation and the application for infrared dim small target detection," *Pattern Recognit.*, vol. 43, no. 6, pp. 2145–2156, Jun. 2010.
[13] S. D. Deshpande, M. H. Er, R. Venkateswarlu, and P. Chan, "Max-mean and max-median filters for detection of small targets," *Proc. SPIE*, vol. 3809, pp. 74–83, Jul. 1999.
[14] Y. Q. Zeng and Q. Chen, "Dim and small target background suppression based on improved bilateral filtering for single infrared image," *Infr. Technol.*, vol. 33, no. 9, pp. 537–540, 2011.
[15] T.-W. Bae, "Small target detection using bilateral filter and temporal cross product in infrared images," *Infr. Phys. Technol.*, vol. 54, no. 5, pp. 403–411, Sep. 2011.
[16] X. Hou and L. Zhang, "Saliency detection: A spectral residual approach," in *Proc. IEEE Conf. Comput. Vis. Pattern Recognit.*, Minneapolis, MN, USA, Jun. 2007, pp. 1–8.
[17] T. Liu and X. Li, "Infrared small targets detection and tracking based on soft morphology top-hat and SPRT-PMHT," in *Proc. 3rd Int. Congr. Image Signal Process.*, Yantai, China, Oct. 2010, pp. 968–972.
[18] A. Mahalanobis, R. R. Muise, S. R. Stanfill, and A. Van Nevel, "Design and application of quadratic correlation filters for target detection," *IEEE Trans. Aerosp. Electron. Syst.*, vol. 40, no. 3, pp. 837–850, Jul. 2004.
[19] S. Kim, "High-speed incoming infrared target detection by fusion of spatial and temporal detectors," *Sensors*, vol. 15, no. 4, pp. 7267–7293, Mar. 2015.
[20] Z. Liu, C. Chen, X. Shen, and X. Zou, "Detection of small objects in image data based on the nonlinear principal component analysis neural network," *Proc. SPIE*, vol. 44, no. 9, pp. 403–409, Sep. 2005.
[21] Y. Bi, X. Bai, T. Jin, and S. Guo, "Multiple feature analysis for infrared small target detection," *IEEE Geosci. Remote Sens. Lett.*, vol. 14, no. 8, pp. 1333–1337, Aug. 2017.
[22] C. Yang, J. Ma, S. Qi, J. Tian, S. Zheng, and X. Tian, "Directional support value of Gaussian transformation for infrared small target detection," *Appl. Opt.*, vol. 54, no. 9, pp. 2255–2265, Mar. 2015.
[23] J. Mairal, M. Elad, and G. Sapiro, "Sparse representation for color image restoration," *IEEE Trans. Image Process.*, vol. 17, no. 1, pp. 53–69, Jan. 2008.
[24] J. Zhao, Z. Tang, J. Yang, and E. Liu, "Infrared small target detection using sparse representation," *J. Syst. Eng. Electron.*, vol. 22, no. 6, pp. 897–904, Dec. 2011.
[25] W. Zhang, M. Cong, and L. Wang, "Algorithms for optical weak small targets detection and tracking: Review," in *Proc. Int. Conf. Neural Netw. Signal Process.*, Nanjing, China, vol. 1, Dec. 2003, pp. 643–647.
[26] B. Wang, L. Dong, M. Zhao, H. Wu, and W. Xu, "Texture orientation-based algorithm for detecting infrared maritime targets," *Appl. Opt.*, vol. 54, no. 15, pp. 4689–4697, 2015.
[27] L. Zhang, L. Peng, T. Zhang, S. Cao, and Z. Peng, "Infrared small target detection via non-convex rank approximation minimization joint $l_{2,1}$ norm," *Remote Sens.*, vol. 10, no. 11, p. 1821, Nov. 2018.
[28] H. Zhang, L. Zhang, D. Yuan, and H. Chen, "Infrared small target detection based on local intensity and gradient properties," *Infr. Phys. Technol.*, vol. 89, pp. 88–96, Mar. 2018.

YUHANG JIANG received the B.S. degree in optoelectronic information science and engineering from Dalian Maritime University, Dalian, China, in 2018, where he is currently pursuing the joint M.S. degree. His research interests include image super-resolution, small target detection, and image enhancement through digital image processing.

LILI DONG (Member, IEEE) was born in Qitaihe, Heilongjiang, China, in 1980. She received the B.S. degree in mechanical design manufacturing and automation and the M.S. degree from the College of Information Science and Technology, Dalian Maritime University (DLMU), Dalian, China, in 2002 and 2004, respectively, and the Ph.D. degree in instrument science and technology from the Harbin Institute of Technology, Harbin, China, in 2008. From 2005 to 2008, she was a Teaching Assistant with the College of Information Science and Technology, DLMU. From 2008 to 2012, she was a Lecturer with the College of Information Science and Technology, DLMU. Since 2012, she has been an Assistant Professor with the Mechanical Engineering Department. She has authored 13 papers and three inventions. Her research interests include multispectral target recognition, tunnel lighting, and photoelectric detection.

YANG CHEN received the B.S. degree in electronic information engineering from Dalian Ocean University, Dalian, China, in 2017. She is currently pursuing the joint M.S. degree with Dalian Maritime University. Her research interests include object detection and image enhancement through digital image processing.

WENHAI XU received the B.S. and M.S. degrees in precision instrument and the first Ph.D. degree in precision instrument from the Harbin Institute of Technology, Harbin, China, in 1982, 1984, and 1991, respectively, and the second Ph.D. degree in manufacturing machine from the Tokyo Institute of Technology, Tokyo, Japan, in 1993. From 1986 to 1988, he was a Lecturer with the Harbin Institute of Technology and an Assistant Professor, from 1992 to 2001. He has been a Professor with the Harbin Institute of Technology for four years, since 2001. He was the Project Director with Cannon Inc., Tokyo, from 1993 to 2003. He was also a Research Scientist with System Engineers Company Ltd., Yamato, Japan, from 1995 to 1997. He is currently a Professor of opt-electric information science and engineering with Dalian Maritime University, Dalian, China. In the last ten years, he has directed over 30 research projects and applied ten national patents. He has authored over 80 research papers. His research interests include infrared detection, digital image processing, design of high-resolution optical imaging systems, and opt-electronic information processing.